

NJC

New Journal of Chemistry

Accepted Manuscript

A journal for new directions in chemistry

This article can be cited before page numbers have been issued, to do this please use: R. AHMED, A. Ali, M. Ahmad, A. Alsalmeh, R. A. Khan and F. Ali, *New J. Chem.*, 2020, DOI: 10.1039/D0NJ03422C.



This is an Accepted Manuscript, which has been through the Royal Society of Chemistry peer review process and has been accepted for publication.

Accepted Manuscripts are published online shortly after acceptance, before technical editing, formatting and proof reading. Using this free service, authors can make their results available to the community, in citable form, before we publish the edited article. We will replace this Accepted Manuscript with the edited and formatted Advance Article as soon as it is available.

You can find more information about Accepted Manuscripts in the [Information for Authors](#).

Please note that technical editing may introduce minor changes to the text and/or graphics, which may alter content. The journal's standard [Terms & Conditions](#) and the [Ethical guidelines](#) still apply. In no event shall the Royal Society of Chemistry be held responsible for any errors or omissions in this Accepted Manuscript or any consequences arising from the use of any information it contains.

Phenanthroimidazole derivatives as Chemosensor for Picric Acid: A First Realistic

View Article Online
DOI: 10.1039/C5NJ03422C

Approach

Ruby Ahmed^a, Abid Ali^a, Musheer Ahmad^a, Ali Alsalmeh^b, Rais Ahmad Khan^{*b}, and

Farman Ali^{*a}

^a Department of Applied Chemistry, Zakir Hussain College of Engineering and Technology, AMU, Aligarh 202002. Email: farmanfrequent@gmail.com, amusheer4@gmail.com, abidaliamu4@gmail.com, ahmedruby1974@gmail.com

^b Department of Chemistry, College of Sciences, King Saud University, P.O. Box 2455, Riyadh, 11451, KSA. Email: aalsalme@ksu.edu.sa and krais@ksu.edu.sa

Abstract:

A series of phenanthroimidazole (PI) derivatives (M1-M3): 2-phenyl-1H-phenanthro [9,10-d]imidazole (M1), 2-anthryl-1H-phenanthro[9,10-d]imidazole (M2), 2-pyrenyl-1H-phenanthro[9,10-d]imidazole (M3) were synthesized and characterized using various spectroscopic techniques. The fluorescence quenching studies or sensing properties of the molecules M1-M3 with picric acid (PA) were studied. The molecules (M1-M3) exhibit strong fluorescence with peak emission wavelength at 386, 486 and 456 nm. This emission gets quenched with the addition of PA. The mechanism of fluorescence quenching involves proton transfer from PA to M in the ground state, followed by complex formation between cation (M⁺) and picrate anion (PA⁻). The proton transfer breaks the conjugation inside the imidazole ring which in turn leads to loss of fluorescence. The proof of proton transfer was evident from single X-ray crystal structure of the co-crystals (M1⁺-PA⁻ and M3⁺-PA⁻) and their Hirshfeld surface analysis. Time-resolved fluorescence measurements reveal that quenching is static. The complex formation constant (K_s) and life-time for all the molecules is measured.

Introduction

View Article Online
DOI: 10.1039/D0NJ03422C

Environmental pollution is a major concern in the present century. The increasing use of chemicals in our modern life is deteriorating the water bodies and agricultural lands^{1,2}. 2,4,6-trinitrophenol, also known as picric acid (PA), is also one such chemical used in the dye industry, pharmaceuticals and chemical industries^{3,4}. It is soluble in water and does not degrade easily. It affects liver functions, respiratory systems, fertility and also causes anaemia, eye irritation and cancer^{5,6}. It is also recognized as a more powerful explosive material than its structural analogous like trinitrotoluene (TNT) and p-dinitrobenzene (p-DNB) etc⁷. PA can easily be used by terrorists for unlawful activities. Therefore, its specific and sensitive detection is desirable.

The conventional method utilized for PA detection has a long list of techniques such as gas chromatography-mass spectrometry (GC-MS), electrochemistry, surface-enhanced Raman spectroscopy, four-probe conductivity measurement and so on⁷⁻¹¹. Amongst these, the fluorescence is more attractive for the following reasons. Firstly, the photomultiplier (PMT) detectors of fluorimeter are very sensitive therefore; it requires a small sample for signal detection. Also, the technique is cost-effective and involves fast signal processing. Many fluorescent sensors of PA have been reported. It includes metal-organic frameworks, nanoparticles, fluorescence upconversion materials, azo dyes, derivatives of oxadiazoles, tetrazoles, histidines and squaraines etc^{8,11-19}. The sensing mechanism for PA depends on the nature of probe²⁰. The sensing mechanism of nitrogen-containing heterocycles like histidine or oxidazole was mainly ascribed to proton transfer and energy transfer.

To the best of our knowledge, the proof of proton transfer from PA to a nitrogen atom of the heterocycle has not been demonstrated in the literature. Also, it is the first report of using phenanthroimidazole for detecting PA. Phenanthroimidazole is a planar and rigid aromatic system. It exhibits significantly good electron transport and photophysical properties. It also

has good thermal stability. Due to these properties, phenanthroimidazole derivatives find their use as fluorophores for laser dyes, probe for cysteine and homocysteine, component for red, green and blue (RGB) emitting systems in organic light-emitting devices (OLEDs) etc^{21–25}. Herein we demonstrate the phenanthroimidazoles as a family of compounds for which fluorescence get quenched with the addition of PA and also explore the mechanism of photoluminescence quenching (PLQ) by growing crystal of complex of M1 and PA i.e., $M1^+-PA^-$ and crystal of complex M3 and PA i.e. $M3^+-PA^-$.

Experimental Section

Chemicals and Instrumentations

Phenanthrene-9,10-dione (Merck), Benzaldehyde (Merck), 9-anthraldehyde (Merck), and 1-Pyrenecarboxaldehyde (Merck), Picric acid (Merck), glacial acetic acid (Merck), Ammonium acetate (Merck) and ethanol (Merck) were used as received. Perkin Elmer IR spectrometer was used to record Fourier-transform infrared spectra. UV-Vis spectral measurements were carried out using Perkin Elmer LAMBDA-45 spectrophotometer. The Florescence spectra were obtained by a HITACHI-F2500 spectrofluorimeter. Melting points were measured in Mel Temp device using sealed capillaries. The 1H and ^{13}C NMR spectra were recorded at room temperature using a Bruker 300 MHz NMR spectrometer.

The Single X-ray measurements for Co-crystals ($M1^+-PA^-$) and ($M3^+-PA^-$) were carried out on a Bruker APEX II Kappa CCD single crystal diffractometer equipped with a graphite monochromator. $MoK\alpha$ radiation ($\lambda = 0.71073 \text{ \AA}$) was used for the collection, which was controlled by APEX2 with data collected at 100(2)K. Using Olex2²⁶, the structure was solved with the olex2.solve²⁷ structure solution program using Charge Flipping and refined with the olex2.refine²⁷ refinement package using Gauss-Newton minimisation. Masking refinement has

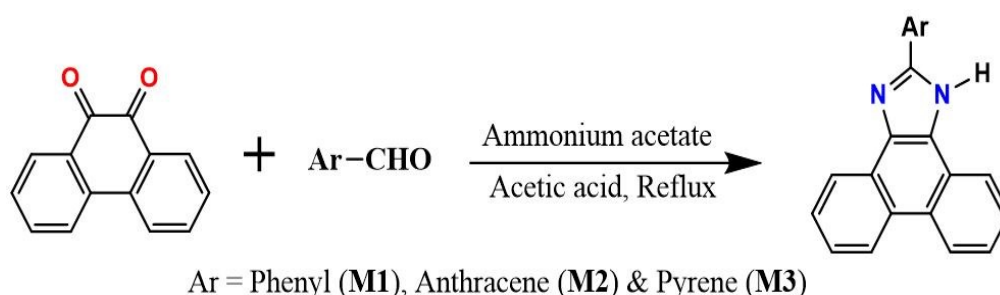
been done in (M3⁺-PA⁻) as the electron densities corresponding to one lattice DMSO molecules are highly diffused.

Squeezed refinement has been done as the electron densities corresponding to two crystallised lattice DMSO molecules are highly diffused.

Results and discussion

General Procedure of the Synthesis of the Compounds

The molecules M1, M2, and M3 were synthesized using the reported procedure as shown in scheme 1²⁴. It involves a one-step condensation reaction between equimolar quantities of phenanthrene-9,10-dione and aryl aldehyde. 1 mmole of phenanthrene-9,10-dione, 1 mmole of aryl aldehyde and 5 mmoles of ammonium acetate were added to single-neck 100 ml round-bottom flask. Then 30 ml of glacial acetic acid was added. The mixture was refluxed on magnetic stirred for 12 hours under nitrogen. After completion of the reaction, the reaction mixture was cooled to room temperature and then 50 ml of de-ionized cold water was added. The product formed precipitates out as pale brown solid. The solid product was filtered under suction and was washed thrice with de-ionized water. This was dried in a vacuum oven to give 2- aryl-1-H-phenanthro[9,10 d] imidazole as the final product. (See SI, for FTIR spectra, ¹H, ¹³C NMR)



Scheme 1: Synthesis of compounds M1, M2, and M3.

The crystal of complex (M1⁺-PA⁻) was synthesized by mixing M1 (20 mg) and PA (20 mg) in 5 ml ethanol. This solution was left undisturbed and slow evaporation of the solvent leads to

1
2
3 crystallization. Small crystals were obtained after ten days. The crystal of complex (M3⁺-PA⁻)
4 was synthesized by mixing M3 (100 mg) and PA (300 mg) in 20 ml ethanol and 3 ml DMSO.
5
6 The resulting solution was heated at 70 °C. It was left undisturbed and crystals of M3⁺-PA⁻
7
8 were obtained by slow evaporation of the solvent. The suitable single crystals of M2⁺-PA⁻ was
9
10 not obtained despite of several attempts.
11
12
13

14 **Photophysical Characterization**

15
16 Figure 1a shows the absorption spectra of M1, M2, and M3 in ethanol. All the molecules absorb
17
18 UV light below 450 nm. The peak absorption wavelengths for M1 are at 260, 310, 343 and 360
19
20 nm. The peak absorption wavelengths for M2 are at 249, 275, 303 364 and 384 nm. The peak
21
22 absorption wavelengths for molecule M3 are at 253, 274, 304 and 367 nm. The absorption
23
24 spectra of M2 and M3 are shifted to longer wavelengths than the absorption of M1. Figure 1b
25
26 shows the absorption spectra of M1, PA and complex M1⁺-PA⁻ in ethanol. The absorption of
27
28 the M1⁺-PA⁻ complex is not the superposition of the absorption of its constituent M1 and PA.
29
30 The peak position and relative intensities are not as expected. This reflects an interaction
31
32 between M1 and PA which has been confirmed in the crystal structure of the complex (M1⁺-
33
34 PA⁻). The photoluminescence emission spectrum of M1, M2 and M3 in ethanol is shown in
35
36 Figure 1c. The samples were excited at 340 nm and the emission was monitored between 370
37
38 to 650 nm. The peak emission wavelengths for M1, M2 and M3 are at 386 nm, 486 nm and
39
40 456 nm respectively. The redshift in the absorption and emission was observed with the
41
42 increase in the size of aryl groups. It shows that the optical band gap decreases with the increase
43
44 in π -electrons conjugation.
45
46
47
48
49
50
51
52
53
54
55
56
57
58
59
60

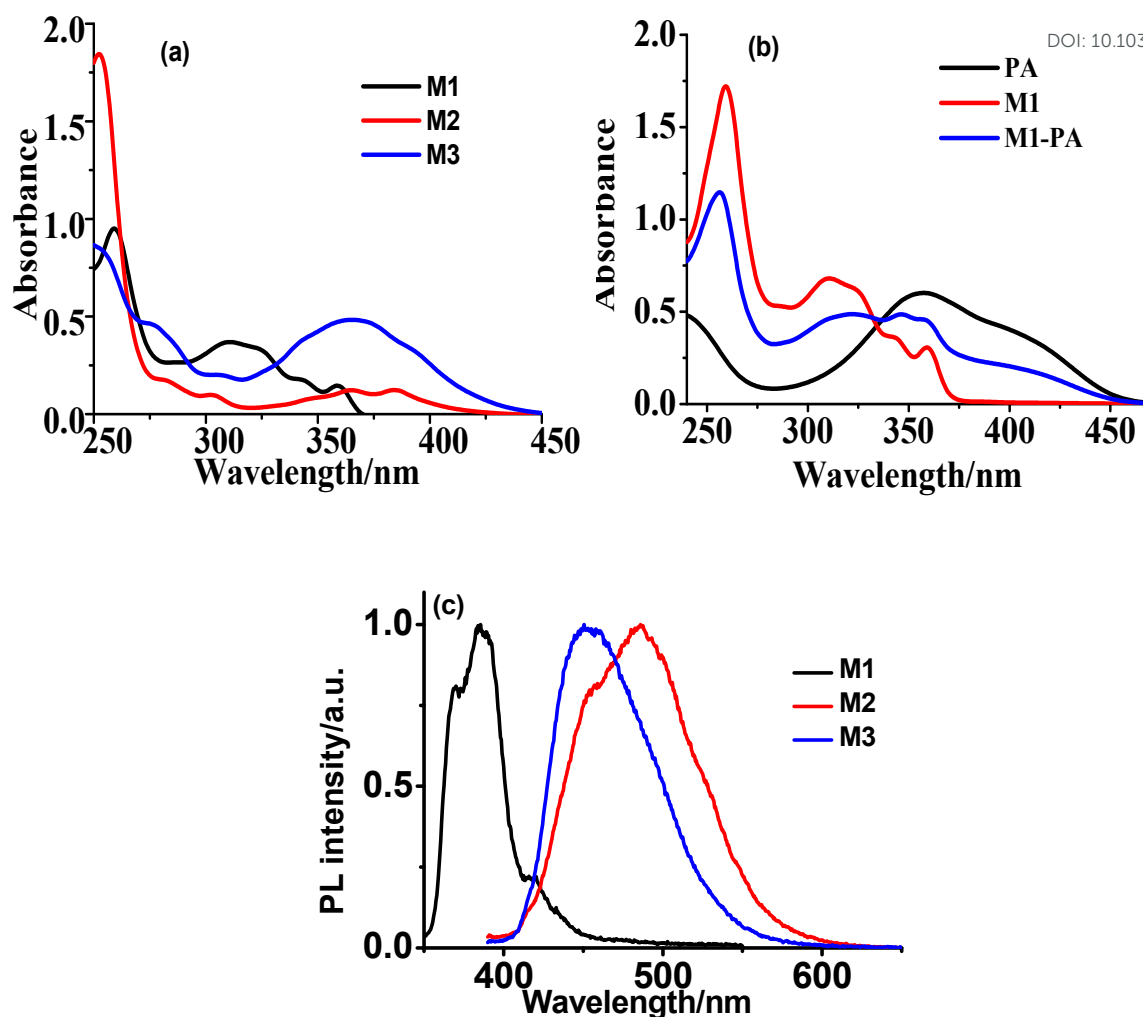


Figure 1(a). The absorption spectra of M1 M2 and M3 recorded in ethanol. **(b)** Absorption spectra of M1, PA, and complex (M1⁺-PA⁻). **(c)** The photoluminescence (PL) emission spectrum of M1, M2, and M3 recorded in ethanol.

Structural Description of (M1⁺-PA⁻)

Figure 2 shows the molecular structure of the synthesized co-crystal. The space group of the co-crystal is Triclinic, P-1. This incorporates two molecules of M1, two molecules of picric acid and one water molecule in an unsymmetrical unit. The process of crystallization begins

with proton transfer from the hydroxyl group of picric acid to the nitrogen atom of the imidazole ring in M1. The water molecule then assists in the co-crystal formation. One hydrogen atom of water molecule undergoes hydrogen bond interaction with the oxygen atom of the hydroxyl group in picric acid and the other hydrogen atom with the oxygen atom from the nitro group of another picric acid. The oxygen atom of the same water molecule interacts with N-H of imidazole in M1 via H-bonding. Thus, all atoms of water are engaged in H-bonding interaction with the two picric acids and one imidazole of M1. A detailed topology of the complex $\mathbf{M1}^+ - \mathbf{PA}^-$ is also presented in supporting information.

Next Article Online
DOI: 10.1039/C9NJ03422C

1
2
3
4
5
6
7
8
9
10
11
12
13
14
15
16
17
18
19
20
21
22
23
24
25
26
27
28
29
30
31
32
33
34
35
36
37
38
39
40
41
42
43
44
45
46
47
48
49
50
51
52
53
54
55
56
57
58
59
60

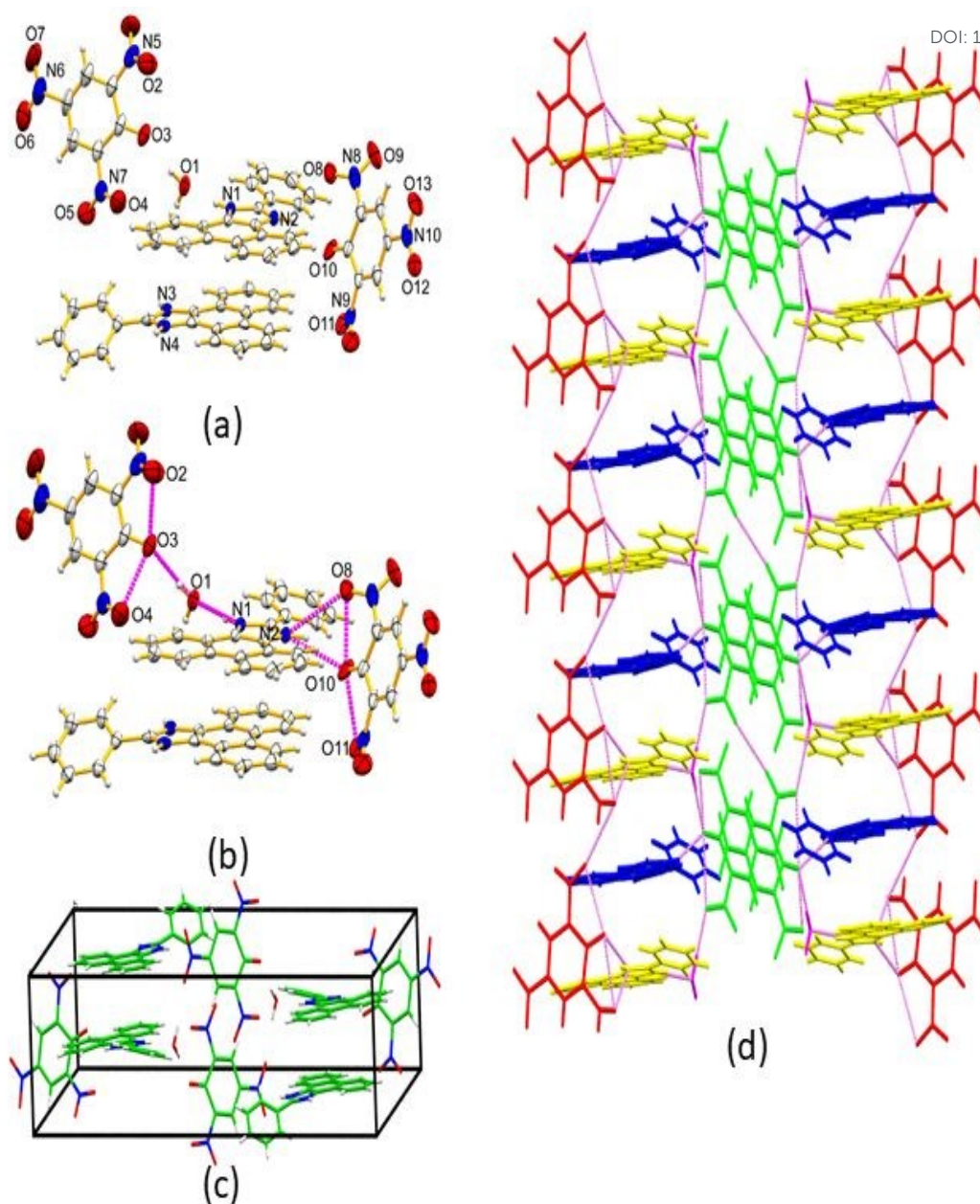


Figure 2(a)Structure of a single crystal $M1^+-PA^-$.(b) Hydrogen bonding's in co-crystals.(c)Crystal packing and (d)supramolecularassembly.

Structural Description of ($M3^+-PA^-$)

Figure 3 shows the molecular structure of the co-crystal $M3^+-PA^-$. The space group of the co-crystal is monoclinic, $P2_1/c$. This incorporates a molecule of $M3$, a molecule of PA and a molecule of the solvent $DMSO$ in an unsymmetrical unit. The process of crystallization begins with the formation of PA anion and $M3$ cation during proton transfer from hydroxyl of picric

acid into the nitrogen of 2-pyrenyl-1H-phenanthro[9,10-d]imidazole. Besides hydrogen bonding, π - π -interactions play an important role in structure formation. The π - π bonds between two M3 cations. Intermolecular contacts M3 – M3 is stronger than DMSO–M3.

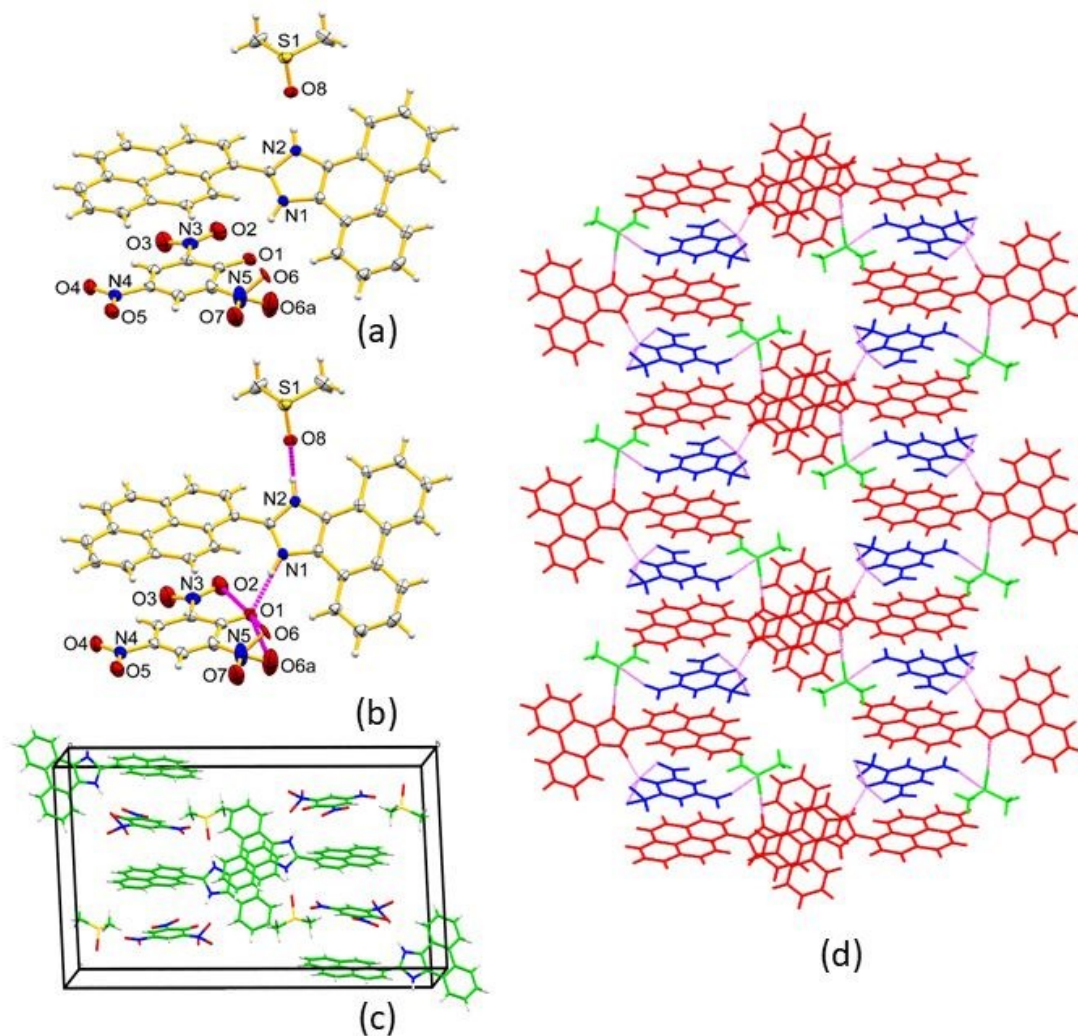


Figure 3(a) Single X-ray Crystal Structure of $M3^+ \cdot PA^-$. (b) Hydrogen bonding in the co-crystals. (c) Crystal packing and (d) Supramolecular Assembly.

Figure 3 shows the molecular structure of the synthesized co-crystal. The space group of the co-crystal is Monoclinic, $P2_1/c$. This incorporates two molecules of 2-pyrene-1H-phenanthro[9,10d]imidazole, two molecules of picric acid and one DMSO molecule in an asymmetric unit.

Table 1: The Crystal Data for Co-crystals, **M1⁺-PA⁻** and **M3⁺-PA⁻**.

Parameters	M1 ⁺ -PA ⁻	M3 ⁺ -PA ⁻
Empirical formula	C ₂₇ H ₁₉ N ₅ O ₈	C ₃₉ H ₂₇ N ₅ O ₈ S
Formula weight	541.48	725.74
Temperature (K)	100(2)	100
Crystal system	Triclinic	Monoclinic
Space group	<i>P</i> 1	<i>P</i> 2 ₁ / <i>c</i>
<i>a</i> (Å)	7.1550(7)	7.4343(5)
<i>b</i> (Å)	13.5698(12)	30.238(2)
<i>c</i> (Å)	13.6958(13)	16.0736 (11)
α (°)	115.283(3)	90
β (°)	100.531(3)	98.342(2)
γ (°)	94.796(3)	90
Volume (Å ³)	1162.41(19)	3575.1(4)
<i>Z</i>	2	4
ρ_{calc} (mg/m ³)	1.5469	1.348
μ (mm ⁻¹)	0.117	0.152
<i>F</i> (000)	560.3	1505.3
Crystal size (mm ³)	0.38 × 0.28 × 0.16	0.39 × 0.28 × 0.17
Radiation	Mo K α (λ = 0.71073)	Mo K α (λ = 0.71073)
2 θ range for data collection (°)	5.76 to 50.1	5.54 to 50.1
Index ranges	-9 ≤ <i>h</i> ≤ 9, -18 ≤ <i>k</i> ≤ 18, -18 ≤ <i>l</i> ≤ 18	-9 ≤ <i>h</i> ≤ 9, -40 ≤ <i>k</i> ≤ 40, -21 ≤ <i>l</i> ≤ 21
Reflections collected	18582	57453
Independent reflections	4119 (<i>R</i> _{int} = 0.0904, <i>R</i> _{sigma} = 0.1035)	6312 (<i>R</i> _{int} = 0.0779, <i>R</i> _{sigma} = 0.0536)
Data/restraints/parameters	4119/0/364	6312/0/595
Goodness-of-fit on <i>F</i> ²	1.110	1.091
Final <i>R</i> indexes [<i>I</i> ≥ 2 σ (<i>I</i>)]	<i>R</i> ₁ = 0.0545, <i>wR</i> ₂ = 0.1193	<i>R</i> ₁ = 0.0453, <i>wR</i> ₂ = 0.1100
Largest diff. peak/hole / e Å ⁻³	0.40/-0.46	0.50/-0.42
Final <i>R</i> indexes [all data]	<i>R</i> ₁ = 0.0889, <i>wR</i> ₂ = 0.1445	<i>R</i> ₁ = 0.0611, <i>wR</i> ₂ = 0.1234
CCDC	1981809	1981808

^aGOF is defined as $\{\sum[w(F_0^2 - F_c^2)]/(n - p)\}^{1/2}$ where *n* denotes the number of data pieces and *p* the number of parameters. ^b*R* = $\{\sum\|F_0| - |F_c|\} / \sum|F_0|$, *wR*₂ = $\{\sum w(F_0^2 - F_c^2)^2 / \sum w(F_0^2)\}^{1/2}$

The phenanthrene imidazole rings of the molecule of 2-pyrenel-1H-phenanthro[9,10d]imidazole are planar and bear a torsional angle of 43.39 (N1-C15-C16-C29) with the pyrene unit of the molecule of 2-pyrene-1H-phenanthro[9,10d]imidazole. The molecule is stabilized by hydrogen bonds. The prominent ones are between O8-H2 (molecules of DMSO and imidazole ring H2 of M3), O1---H1(between H1 of imidazole and O1 of PA) and intramolecular hydrogen bonds between phenolic O1 and ortho nitro groups of PA. These are

The red spots in the Hirshfeld surface of M1 (figure 4) are centered at N1-H1, N2-H2, C11-H11, C40-H40, C36-H36, C41-H41, C33-H33, C34-H34. All the atoms of water molecules are involved in H-bonding interactions. The oxygen atom of water molecule interacts with C-H bonds of phenyl and phenanthrene and also with the N-H of imidazole ring in M1. The percentage contributions of H---H and H---O contacts are 32.7% and 23.2% of the total d_{norm} surface of $M1^+$ (Figure 4a).

The N-H---O interaction appears as a sharp spike on the two-dimensional fingerprint plot of H---O contacts. The percentage contribution of various interactions is shown in the fingerprint (FP) plot. Analysis of the Hirshfeld surface of $M1^+$ (type 2) is shown in figure 5. The dark red spot showing strong hydrogen-bonding interaction is centered at N3-H3.

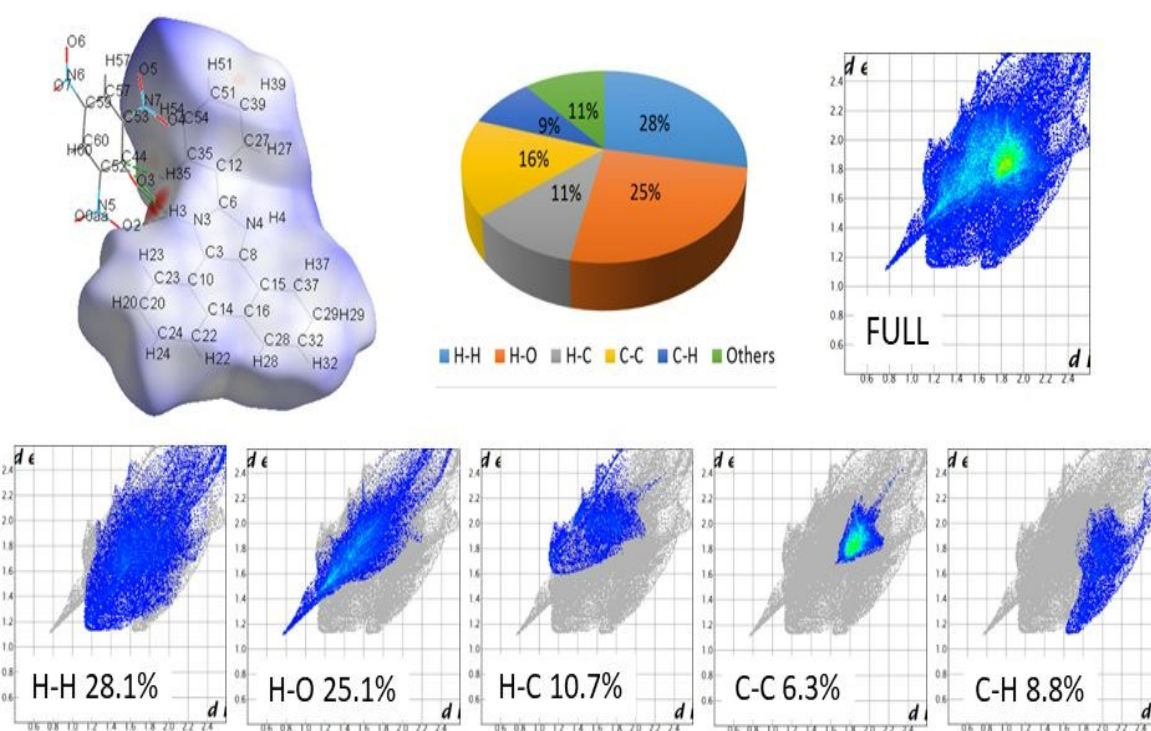


Figure 5. Hirshfeld surface for M1 (type 2) with d_{norm} over the range of -0.57 to 2.74. Neighboring molecules (PA) associated with close contacts are also shown. Pie chart and FP for overall, other contacts and percentage contribution from different contacts in M1.

The pie chart in figure 5 shows the percentage contribution of various interactions in the complex. The percentage contribution of H---H and H---O is 28.1% and 25.1% respectively. The H---O interaction includes oxygen atoms from the nitro and phenoxide groups in PA⁻. The sharp peak in the FP plot of H---O contacts corresponds to N3-H3---O3 i.e., hydrogen from the nitrogen of imidazole and oxygen from the phenoxide group in PA⁻. Hirshfeld surface analysis of complex **M3**⁺-PA⁻ is discussed in supporting information.

Sensing Studies

Stock solutions of 10 mM concentration were made for different metal ions and nitroaromatic compounds. The tested metal ions include Na⁺, Cu²⁺, Mg²⁺, Fe²⁺, Cd²⁺, and nitroaromatic compounds include 2-nitrotoluene, trinitrotoluene, dinitrobenzene, and picric acid. The synthesized molecules M1, M2 and M3, were soluble in chloroform and ethanol. The samples were excited at 340 nm and emission was monitored. The sensing abilities of M1-M3 in ethanol were investigated for the above-mentioned metal ions. We find no change in the peak position and intensity of emission in the fluorescence spectra of M1-M3. Then nitro-aromatics were tested for their sensing. Among the tested nitroaromatics, only PA showed quenching in the fluorescence intensity. Phenols and aromatic acids were also found to quench the fluorescence. Figure 6 shows the photoluminescence quenching of M1, M2 and M3 with the successive addition of PA as a quencher. The fast and selective quenching was observed for PA among the tested nitroaromatics. The formation constants (K_s) were calculated using the equation.

$$F_0/F = 1 + K_s[Q]$$

Where F and F₀ are the fluorescence intensity with and without quencher, respectively, K_s is the ground state complex formation constant (litre/mole) for static quenching and [Q] is the quencher concentration (mole/litre). The fluorescence intensities were measured at the peak emission wavelengths. The K_s is calculated from the slope of the linear fit between the

quenching and quencher concentration (Figure 6). Table 2 summarizes the values of K_s for M1-M3. The K_s values of M1-M3 are high and nearly similar. We find no correlation between the size of aryl group and formation constant. As revealed from the Hirschfeld surface analysis of $M1^+-PA^-$ and $M3^+-PA^-$, the stronger interactions in the complexes are centred on the nitrogen atoms, terminal carbon of phenanthrene and terminal carbons of aryl groups. The other atoms in bigger aryl group contribute less with weak Van der waal forces. Therefore, we see less of effect on the formation constant with the size of aryl groups. The above equation is similar to the Stern-Volmer equation except that it gives formation constant rather than Stern-Volmer constant which is related to dynamic quenching. The limit of detection (LOD) for M1-M3 are 0.64, 0.53 and 1.05 ppm respectively. These values are comparable to the values reported in literature for nitrogen containing compounds like histidines, anthracene bridged poly(N-vinylpyrrolidone), substituted oxadiazoles and tetrazoles²⁸⁻³⁰.

Table 2: The K_s and LOD of molecules M1-M3.

Molecule	K_s (litre/mole)	LOD mole/litre , (ppm)
M1	8.62×10^4	2.8×10^{-6} , 0.64
M2	1.45×10^5	2.3×10^{-6} , 0.53
M3	8.53×10^4	4.6×10^{-6} , 1.05

In literature, the quenching with PA is proposed to be because of resonance energy transfer and proton transfer²⁰⁻²². Herein we rule out the possibility of resonance energy transfer for the following reasons. The molecule M1, M2 and M3 have different emission wavelengths and the overlap of these emissions with the absorption wavelengths is also different. We do not see any correlation between this overlap and the amount of quenching. Secondly, the quenching of fluorescence intensity is related to the proton transfer from the hydroxyl group of PA to the

nitrogen atom of imidazole in phenanthroimidazole derivatives in the ground state. The proton transfer is evident from the solved crystal structure complex $M1^+-PA^-$ (Figure 2). The proton transfer breaks the conjugation in imidazole. The loss of conjugation is evident from the increasing C=N distance from 1.326 Å in M1 to 1.344 Å in $M1^+$ in the complex. The loss of conjugation results in fluorescence quenching. Also, the deprotonation of PA leads to a decrease in C-O distance from 1.344 Å to 1.254 Å (Figure 7). The formation of a non-fluorescent complex in the ground state is confirmed by doing time-resolved fluorescence measurements. Figure 8 shows the lifetime decay of M1, M2 and M3. The average lifetime of excited states of M1, M2 and M3 are measured to be 6.0, 3.9 and 2.0 ns respectively. The lifetime remains unchanged with the addition of PA. The χ^2 value ranges from 0.99 to 1.06 in all three cases.

View Article Online
DOI: 10.1039/C5NJ03422C

1
2
3
4
5
6
7
8
9
10
11
12
13
14
15
16
17
18
19
20
21
22
23
24
25
26
27
28
29
30
31
32
33
34
35
36
37
38
39
40
41
42
43
44
45
46
47
48
49
50
51
52
53
54
55
56
57
58
59
60

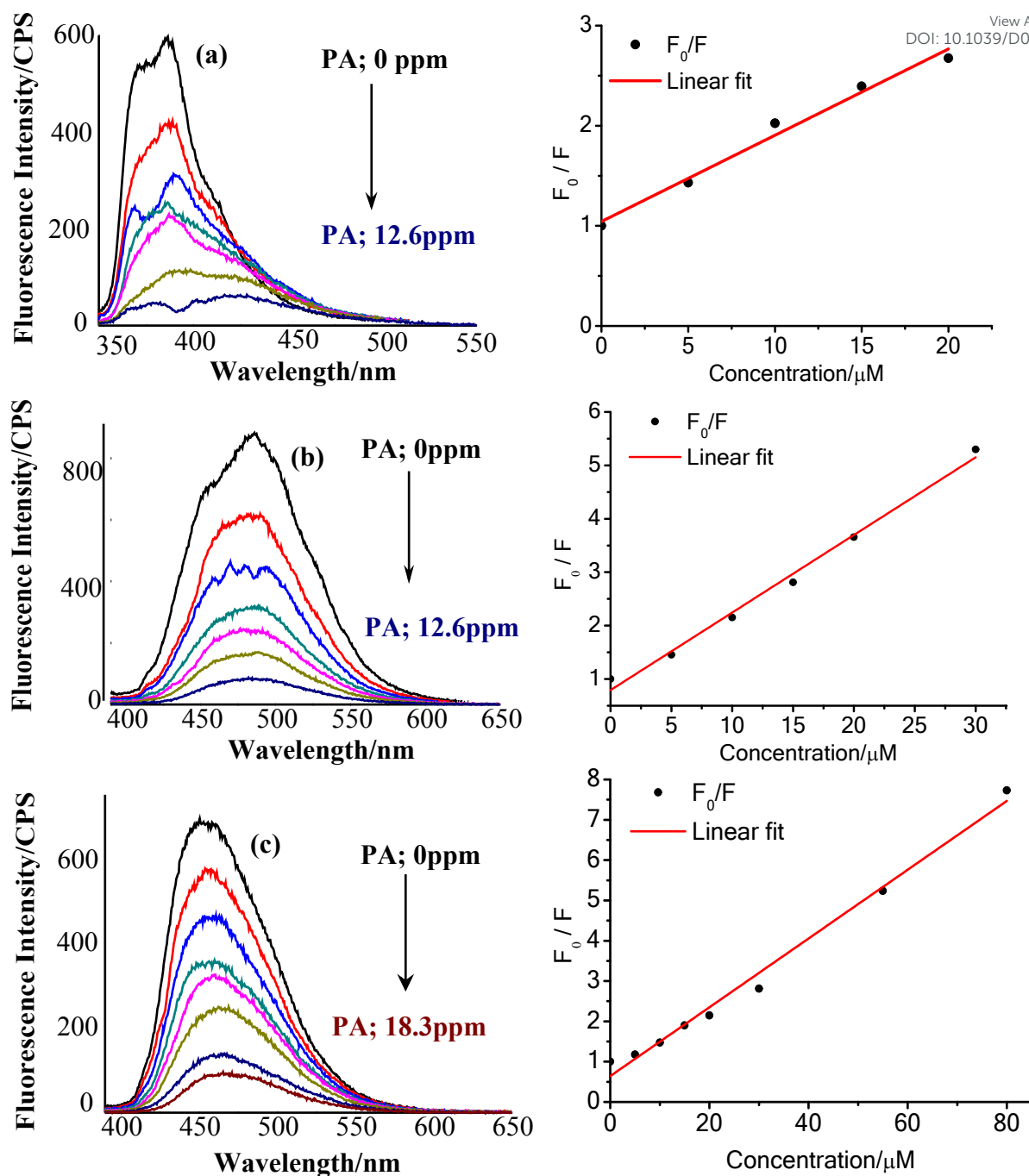


Figure 6. Fluorescence quenching and Stern-Volmer plots upon addition of PA to (a) M1, (b) M2, and (c) M3 respectively.

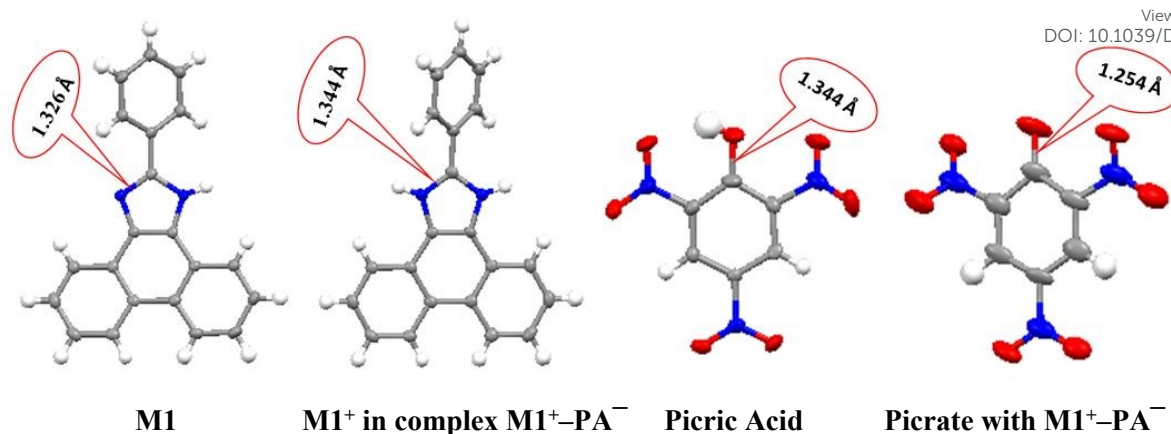


Figure 7. Shows the C=N bond distances in M1, and M1⁺ and also C-O bond distances in PA and PA⁻. The C-O bond length in picric acid (PA) also decreases from 1.344 Å to 1.254 Å with the formation of the anion (PA⁻).

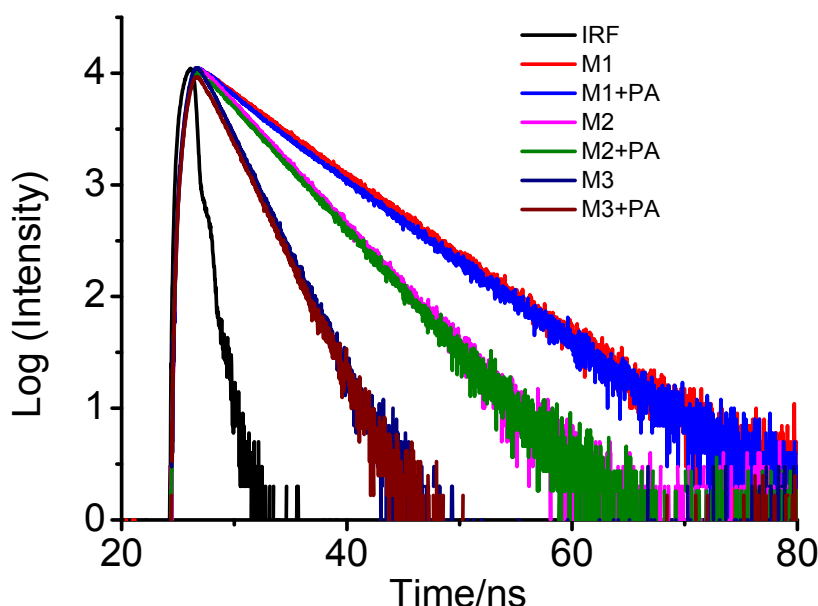


Figure 8. Semi-log plots of fluorescence decay versus time for (M1 and M1⁺-PA⁻), (M2 and M2⁺-PA⁻) and (M3 and M3⁺-PA⁻) in (solvent) at ($\lambda_{\text{ex}} = 397 \text{ nm}$, $\lambda_{\text{em}} = 505 \text{ nm}$).

Conclusion

In summary, a series of phenanthroimidazole (PI) derivatives (M1-M3) were synthesized and characterized. The synthesized compounds give blue emission in ethanol solution and have shown sensing of PA with high sensitivity via fluorescence quenching. The mechanism of quenching involves a proton transfer from the hydroxyl group of PA to Nitrogen atom of

1
2
3 imidazole, followed by complex formation cation ($M1^+$) and picrate anion (PA^-). The proton-
4 transfer results in loss of conjugation. The complex formation has been demonstrated by
5
6 growing the crystal of $M1^+-PA^-$. The selectivity to PA over other tested nitro aromatics is
7
8 because of its deprotonation ability. It provides a rational strategy to design nitrogen containing
9
10 fluorophores of different colours for the sensing of picric acid. To the best of our knowledge,
11
12 this is the first demonstration of fluorescence quenching of PI derivatives with PA. The higher
13
14 value of formation constant is suggestive of the potential of these molecules for pollution
15
16 control and security applications.
17
18
19

Supporting Information:

20
21
22 1H NMR, ^{13}C NMR, FTIR spectra of M1, M2, M3, and Crystallographic data of $M1^+-PA^-$
23
24 (CCDC No 1981809), $M3^+-PA^-$ (CCDC No 1981808), used in this work.
25
26
27

Corresponding Authors:

28
29
30 Dr. Farman Ali, farmanfrequent@gmail.com,
31
32

33
34 Phone: - +91-9758304357
35

ORCID:

36
37
38 **Farman Ali: - 0002-5807-3195**

39
40 **Musheer Ahmad: - 0000-0002-7446-0232**

41
42 **Ruby Ahmed: - 0000-0003-0122-1449**

Conflicts of interest

43
44
45
46
47 "There are no conflicts to declare."
48

Acknowledgments

49
50
51 Dr. Farman Ali acknowledges DST for INSPIRE Faculty funding. Chairman of Department
52
53 of Applied Chemistry, and Director of Interdisciplinary Nanotechnology Centre, A.M.U. for
54
55 allowing the use of fluorimeter. Prof. Ali Alsalmeh would like to acknowledge the Researchers
56
57 Supporting Project (RSP-2020/78), King Saud University, Riyadh, Saudi Arabia.
58
59
60

References

View Article Online
DOI: 10.1039/D0NJ03422C

1. Zhang, Y., Li, F., Zhang, Q., Li, J. & Liu, Q. Science of the Total Environment Tracing nitrate pollution sources and transformation in surface- and ground-waters using environmental isotopes. *Sci. Total Environ.* **490**, 213–222 (2014).
2. Heald, C. L. & Spracklen, D. V. Land Use Change Impacts on Air Quality and Climate. (2015). doi:10.1021/cr500446g
3. S, A. L. Medicinals and Dyes. **18**, 1336–1337
4. Meredith DT, L. C. A Study of Antiseptic Compounds for the Treatment of Burns. *Am. Pharm. Assoc.* **28(6)**, 369–373 (1983).
5. Blackman, W. C. *Basic Hazardous Waste Mangement*. (Lewis, CRC Press LLC, 2001).
6. Wollin, K.-M. & Dieter, H. H. Toxicological Guidelines for Monocyclic Nitro-, Amino- and Aminonitroaromatics, Nitramines, and Nitrate Esters in Drinking Water. *Arch. Environ. Contam. Toxicol.* **49**, 18–26 (2005).
7. Yinon, J. Peer Reviewed: Detection of Explosives by Electronic Noses. *Anal. Chem.* **75**, 98 A-105 A (2003).
8. Holthoff, E. L., Stratis-Cullum, D. N. & Hankus, M. E. A nanosensor for TNT detection based on molecularly imprinted polymers and surface enhanced Raman scattering. *Sensors (Basel)*. **11**, 2700–2714 (2011).
9. Hodyss, R. & Beauchamp, J. L. Multidimensional Detection of Nitroorganic Explosives by Gas Chromatography-Pyrolysis-Ultraviolet Detection. *Anal. Chem.* **77**, 3607–3610 (2005).
10. Ahmed, S. M., Patil, R. C., Nakayama, M. & Ogura, K. Characterization of picric-acid-doped poly(o-toluidine) and the picric-acid-doped poly(o-toluidine)-induced conductive composite of acrylonitrile–butadiene–styrene. *Synth. Met.* **114**, 155–160

(2000).

View Article Online
DOI: 10.1039/D0NJ03422C

11. Pal, A., Sk, M. P. & Chattopadhyay, A. Conducting Carbon Dot–Polypyrrole Nanocomposite for Sensitive Detection of Picric acid. *ACS Appl. Mater. Interfaces* **8**, 5758–5762 (2016).
12. Hirshfeld, F. L. Bonded-Atom Fragments for Describing Molecular Charge Densities. *J. Am. Chem. Soc.* **99**, 1271–1276 (1977).
13. Ahamad, M. N., Shahid, M., Ahmad, M. & Sama, F. Cu(II) MOFs Based on Bipyridyls: Topology, Magnetism, and Exploring Sensing Ability toward Multiple Nitroaromatic Explosives. *ACS Omega* **4**, 7738–7749 (2019).
14. Mako, T. L., Racicot, J. M. & Levine, M. Supramolecular Luminescent Sensors. *Chem. Rev.* **119**, 322–477 (2019).
15. Xu, Y. *et al.* “ICT-not-quenching” near infrared ratiometric fluorescent detection of picric acid in aqueous media. *Chem. Commun.* **49**, 4764–4766 (2013).
16. Nagendran, S., Vishnoi, P. & Murugavel, R. Triphenylbenzene Sensor for Selective Detection of Picric Acid. *J. Fluoresc.* **27**, 1299–1305 (2017).
17. Sanda, S., Parshamoni, S., Biswas, S. & Konar, S. Highly selective detection of palladium and picric acid by a luminescent MOF: a dual functional fluorescent sensor. *Chem. Commun.* **51**, 6576–6579 (2015).
18. Mahata, M. K., Bae, H. & Lee, K. T. Upconversion Luminescence Sensitized pH-Nanoprobes. *Molecules* **22**, 2064 (2017).
19. Mahata, M. K. & Lee, K. T. Development of near-infrared sensitized core–shell–shell upconverting nanoparticles as pH-responsive probes. *Nanoscale Adv.* **1**, 2372–2381 (2019).
20. Tanwar, A. S., Meher, N., Adil, L. R. & Iyer, P. K. Stepwise elucidation of fluorescence based sensing mechanisms considering picric acid as a model analyte.

- Analyst* **145**, 4753–4767 (2020).
21. Tsai, M.-S., Hsu, Y.-C., Lin, J. T., Chen, H.-C. & Hsu, C.-P. Organic Dyes Containing 1H-Phenanthro[9,10-d]imidazole Conjugation for Solar Cells. *J. Phys. Chem. C* **111**, 18785–18793 (2007).
22. Ali, F., Periasamy, N., Patankar, M. P. & Narasimhan, K. L. Integrated Organic Blue LED and Visible–Blind UV Photodetector. *J. Phys. Chem. C* **115**, 2462–2469 (2011).
23. Zhu, J.-J. *et al.* The structure optimization of phenanthroimidazole based isomers with external quantum efficiency approaching 7% in non-doped deep-blue OLEDs. *J. Mater. Chem. C* **8**, 2975–2984 (2020).
24. Kula, S. *et al.* Phenanthro[9,10-d]imidazole with thiophene rings toward OLEDs application. *Dye. Pigment.* **159**, 646–654 (2018).
25. Chen, W.-C., Tong, Q.-X. & Lee, C.-S. The Development of Phenanthroimidazole Derivatives in Blue-Emitting Organic Electroluminescence. *Sci. Adv. Mater.* **7**, (2015).
26. Dolomanov, O. V, Bourhis, L. J., Gildea, R. J., Howard, J. A. K. & Puschmann, H. OLEX2: a complete structure solution, refinement and analysis program. *J. Appl. Crystallogr.* **42**, 339–341 (2009).
27. LJ, B., OV, D., RJ, G., JA, H. & H., P. The anatomy of a comprehensive constrained, restrained refinement program for the modern computing environment - Olex2 dissected. *Acta Crystallogr A Found Adv.* **71**, 59–75 (2015).
28. Singh, R. *et al.* Highly selective fluorescence ‘turn off’ sensing of picric acid and efficient cell labelling by water-soluble luminescent anthracene-bridged poly(N-vinyl pyrrolidone). *Analyst* **144**, 3620–3634 (2019).
29. Nath, S. *et al.* A sensitive and selective sensor for picric acid detection with a fluorescence switching response. *New J. Chem.* **42**, 5382–5394 (2018).
30. Patel, R., Bothra, S., Kumar, R. & Sahoo, S. K. Selective turn-off sensing of picric

acid and p-nitrophenol using fluorescent histidine. *Nano-Structures & Nano-Objects* **19**, 100345 (2019). View Article Online
DOI: 10.1059/DONJ03422C

31. Ponnuvel, K., Banuppriya, G. & Padmini, V. Sensors and Actuators B : Chemical Highly efficient and selective detection of picric acid among other nitroaromatics by NIR fluorescent organic fluorophores. *Sensors Actuators B. Chem.* **234**, 34–45 (2016).
32. Kumar, M., Reja, S. I. & Bhalla, V. LETTERS A Charge Transfer Amplified Fluorescent Hg 2 þ Complex for Detection of Picric Acid and Construction of Logic Functions. 2009–2012 (2012). doi:10.1021/ol3029753
33. Chowdhury, A. & Mukherjee, P. S. Electron-Rich Triphenylamine-Based Sensors for Picric Acid Detection. *J. Org. Chem.* **80**, 4064–4075 (2015).

Phenanthreneimidazole derivatives as Chemosensor for Picric Acid: A First Realistic

View Article Online

DOI: 10.1039/D0NJ03422C

Approach

Ruby Ahmed^a, Abid Ali^a, Rais Ahmad Khan^{*,b}, Ali Alsalmeh^b, Musheer Ahmad^a, and

Farman Ali^{*,a}

^aDepartment of Applied Chemistry, Zakir Hussain College of Engineering and Technology, AMU, Aligarh 202002. Email: farmanfrequent@gmail.com, amusheer4@gmail.com, abidaliamu4@gmail.com, ahmedruby1974@gmail.com

^bDepartment of Chemistry, College of Sciences, King Saud University, P.O. Box 2455, Riyadh, 11451, KSA. Email: krais@ksu.edu.sa and aalsalme@ksu.edu.sa

1
2
3
4
5
6
7
8
9
10
11
12
13
14
15
16
17
18
19
20
21
22
23
24
25
26
27
28
29
30
31
32
33
34
35
36
37
38
39
40
41
42
43
44
45
46
47
48
49
50
51
52
53
54
55
56
57
58
59
60

Graphical Abstract

